# We are IntechOpen, the world's leading publisher of Open Access books Built by scientists, for scientists

**5,300**
Open access books available

**130,000**
International authors and editors

**155M**
Downloads

Our authors are among the

**154**
Countries delivered to

**TOP 1%**
most cited scientists

**12.2%**
Contributors from top 500 universities

CLARIVATE ANALYTICS BOOK CITATION INDEX INDEXED

WEB OF SCIENCE™

Selection of our books indexed in the Book Citation Index in Web of Science™ Core Collection (BKCI)

## Interested in publishing with us?
## Contact book.department@intechopen.com

Numbers displayed above are based on latest data collected.
For more information visit www.intechopen.com

14

# Noise Estimation of Polarization-Encoded Images by Peano-Hilbert Fractal Path

Samia Ainouz-Zemouche[1] and Fabrice Mériaudeau[2]
[1]*Laboratoire d'Informatique, de Traitement de l'Information et des systèmes, (LITIS, EA4108), INSA de Rouen, 76000 Rouen*
[2]*Laboratoire Electronique Informatique et Image (LE2I, UMR CNRS 5158), IUT le Creusot, 71200 Le Creusot*
*France.*

## 1. Introduction

Polarization-sensitive imaging systems have emerged as a very attractive vision technique which can reveal important information about the physical and geometrical properties of the targets. Many imaging polarimeters have been designed in the past for several fields, ranging from metrology (Ferraton et al., 2007), (Morel et al., 2006) to medical (Miura et al., 2006) and remote sensing applications (Chipman, 1993).
Imaging systems that can measure the polarization state of the outgoing light across a scene are mainly based on the ability to build effective Polarization State Analyzers (PSA) in front of the camera enabling to acquire the Stokes vectors (Chipman, 1993), (Tyo et al., 2006). These Stokes polarimeters produced four images called "Stokes images" corresponding to the four Stokes parameters. Accordingly, polarization-encoded images have a multidimensional structure; i.e. multi-component information is attached to each pixel in the image. Moreover, the information content of polarization-encoded images is intricately combined in the polarization channels making awkward their proper interpretation in the presence of noise.
Noise is inherent to any imaging systems and it is therefore present on Stokes images. It is of additive nature when the scene is illuminated by incoherent light and multiplicative when the illumination is coherent (Bénière et al., 2007), (Corner et al., 2003). Its presence degrades the interpretability of the data and prevents from exploring the physical potential of polarimetric information. Few works in the literature addressed the filtering of polarimetric images. We note nevertheless the use of optimization methods by (Zallat et al., 2006) to optimize imaging system parameters that condition signal to noise ratio, or the improvement of the accuracy of the degree of polarization by (Bénière et al., 2007) with the aim of reducing the noise in Stokes images.
The main problem in filtering polarization-encoded images so as to remove their noise content is to respect their physical content. Indeed, mathematical operations which are performed on polarization information images while processing them alter in most cases the physical meaning of the images. The same problem has been encountered for polarization

images segmentation in (Ainouz, 2006a) and (Ainouz, 2006b). Therefore, because of the duality between the polarization images filtering and their physical constraint, a trade-off is to be reached in order to minimize the effect of the noise affecting polarimetric images and to preserve their physical meaning.
In this chapter, we present a technique which, estimate the additive noise (images acquired under incoherent illumination), and eliminate it such that the physical content of the polarimetric images is preserved as much as possible. Our technique combines two methods; Scatter plot (Aiazzi et al., 2002) and data masking (Corner et al., 2003) previously used in the field of multispectral imaging and to take advantage of both them.
As the information content of polarization-encoded images is intricately combined in several polarization channels, Peano-Hilbert fractal path is applied on the noisy image to keep the connectivity of homogeneous areas and to minimize the impact of the outliers. The performances and the bias of our method are statistically investigated by Bootstrap method.
The rest of this chapter is organized as follows: the next section deals with the principle of polarisation images acquisition, the third part details our noise estimation technique whereas part 4 presents the results obtained while filtering polarization encoded images. The chapter ends with a short conclusion.

## 2. Polarization images acquisition

The next two subsections respectively present the principle of a Stoke's imaging system as well as the model for the additive noise resulting from the acquisition set-up.

### 2.1 Stokes imaging

The general polarization state of a light wave can be described by the so called Stokes vector $S$ which fully characterizes the time-averaged polarization properties of a radiation. It is defined by the following combination of complex-valued components $E_x$ and $E_y$ of the electric field, along two orthogonal directions $x$ and $y$ as (Chipman, 1993):

$$S = \begin{pmatrix} S_0 \\ S_1 \\ S_2 \\ S_3 \end{pmatrix} = \begin{pmatrix} \left\langle E_x E_x^* \right\rangle + \left\langle E_y E_y^* \right\rangle \\ \left\langle E_x E_x^* \right\rangle - \left\langle E_y E_y^* \right\rangle \\ 2\,Re\left(\left\langle E_x E_y^* \right\rangle\right) \\ 2\,Im\left(\left\langle E_x E_y^* \right\rangle\right) \end{pmatrix} \tag{1}$$

The first parameter ($S_0$) is the total intensity of the optical field and the other three parameters ($S_1$, $S_2$ and $S_3$) describe the polarization state (Chipman, 1993). $S_1$ is the tendency of the wave to look like a linear horizontal vibration ($S_1$ positive) or a linear vertical vibration ($S_1$ negative). $S_2$ and $S_3$ reflect the nature and the direction of rotation of the wave.
It is straightforward to show that

$$S_0^2 \geq S_1^2 + S_2^2 + S_3^2 \tag{2}$$

This condition is known as the physical condition of Stokes formalism. An arbitrary vector that does not satisfy this condition is not a Stokes vector and doesn't possess any physical meaning.

The general scheme of Stokes images acquisition is illustrated in Figure.1 (Chipman, 1993). The device used for the acquisition is named a classical polarimeter. The wave reflected from the target, represented by a Stokes vector $S_{in}$ , is analyzed by a polarization-state analyzer (PSA) by measuring its projections over four linearly independent states. A PSA consists of a linear polarizer (LP) and a quarter wave (QW) rotating about four angles $(\theta_i)_{i=1,4}$ . Incoming intensities are then measured with a standard CCD camera.

The complete set of 4 measurements can be written in a vectorial form as:

$$I = AS_{in} \tag{3}$$

$I$ is a $4\times1$ intensity matrix measured by the camera. The Stokes vector $S_{in}$ can then easily be extracted from the raw data matrix $I$ provided that the modulation matrix A of the PSA, is known from calibration. For the ideal case (theory), matrix A can be given as (Chipman, 1993):

$$A(\theta_i) = \begin{bmatrix} 1 & -cos^2 2\theta_i & -\frac{1}{2}sin 4\theta_i & sin^2 2\theta_i \\ -1 & cos^2 2\theta_i & \frac{1}{2}sin 4\theta_i & -sin^2 2\theta_i \\ 0 & 0 & 0 & 0 \\ 0 & 0 & 0 & 0 \end{bmatrix} \tag{4}$$

The angles $\theta_i$ are chosen such that the matrix $A$ is invertible to easily recover the Stokes parameters from the intensity matrix. Each of the four intensity component corresponds to one image, leading to four images carrying information about the Stokes vector.

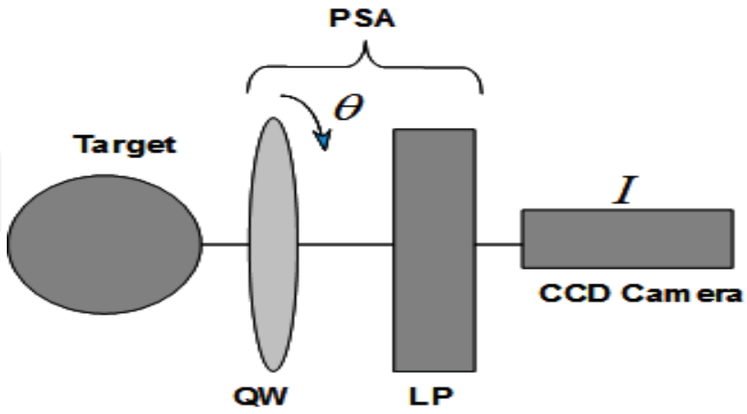


Fig. 1. Stokes imaging device; classical polarimeter

Figure. 2 shows an example of a set of Stokes images obtained with the Stokes imaging device. In order to test the performances of our algorithm, Stokes images were acquired in

strong noisy conditions. In order to have these strong noisy conditions, addition to the natural noise, a hair dryer is turned between the PSA and the camera. The scene is made of 4 small elements of different composition glued on a cardboard. Objects A and D are transparents whereas objects B and C are darks.

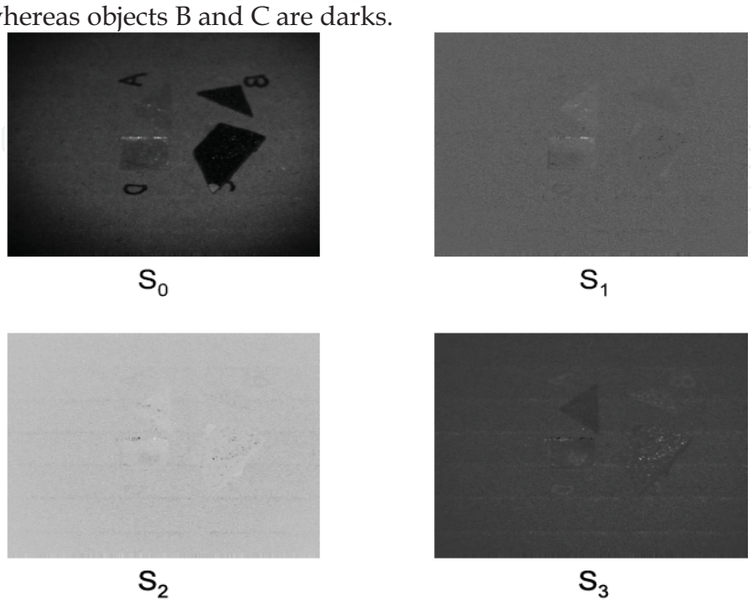


Fig. 2. Stokes image of four small objects glued on a cardboard

The following subsection describes the noise model which was used through out this study.

### 2.1 Noise in Stokes images

It has been established that under incoherent illumination, the noise affecting the images can be modelled as additive and independent (Corner et al., 2003). This type of noise can be modelled by a zero mean random Gaussian distribution which probability density function (PDF) is expressed as follows (Aiazzi et al., 2002):

$$f_x(x) = \frac{1}{\sigma_n \sqrt{2\pi}} exp\left( - \frac{x^2}{2\sigma_n^2} \right) \tag{5}$$

Where $\sigma_n^2$ is the noise variance. The effect of an additive noise $n_a$ on a digital image $g$ at the pixel position $(i, j)$ is expressed as the sum of the noise free image $I$ and the noise in the form :

$$g = I + n_a \tag{6}$$

In perfect acquisition conditions, the Stokes vector is recovered from equation (3) such that:

$$S(i, j) = A^{-1} I(i, j) \tag{7}$$

In the presence of noise, equation (7) becomes:

$$\begin{aligned}\hat{S}(i,j) &= A^{-1}\left(I(i,j)+n_a(i,j)\right)\\ &= A^{-1}I(i,j)+A^{-1}n_a(i,j)\\ &= S(i,j)+\delta S(i,j)\end{aligned} \tag{8}$$

The estimated Stokes vector $\hat{S}$ is an independent sum of the theoretical Stokes vector (noise free) $S$ and the term $\delta S$ due to the additive noise effects. The estimation of the noise distribution is then needed to reconstruct the noisy image $\delta S$ and minimize its effects on the estimated Stokes image $\hat{S}$.

However, as explained above, in the introduction, direct filtering of polarimetric measurements can induce a non physical meaning of the filtered Stokes image $\hat{S}-\delta S$. This means that for an important number of pixels, the vector $\hat{S}-\delta S$ does not satisfy the physical constraint stated in equation (2) and therefore cannot be considered as a Stokes vector which fully fulfils physical constraints. In such conditions, these images have no interest and additional steps have be taken to obtain a trade-off between filtering and physical meaning for as many pixels as possible. The following section presents three methods for noise estimation in the case of additive Gaussian noise.

## 3. Parametric noise estimation

Inasmuch as the estimated noised Stokes image is an independent sum of the noise and the noise free image, the estimation of the $\delta S$ distribution is sufficient to have information about the additive noise. Two multi-spectral filtering methods: Scatter plot method (SP) (Aiazzi et al., 2002) and data masking method (DM) (Corner et al., 2003) were used to process the images. The proposed filtering algorithm takes advantages of both methods.

In order to eliminate the impact of non relevant data, the image is first transformed to a Peano-Hilbert fractal path. This method is applied onto gray level images and the results are compared to the results obtained with SP and DM methods.

### 3.1 Scatter plot and Data masking methods reminder

#### 3.1.1 Scatter plot method (SP)

In the SP method, the standard deviation of the noisy observed image can be evaluated in homogeneous areas (Aiazzi et al., 2002). Under the assumption that the noise is Gaussian with zero mean, local means μ and local standard deviations σ are calculated in a sliding small window within the whole image. The scatter plot plane of local standard deviations (σ) versus local means (μ) is plotted and then partitioned into rectangular blocks of size $L \times L$ ($100 \times 100$ for example). After sorting the blocks by decreasing number of points, denser blocks are considered as the homogeneous areas of the image. The estimated standard deviation of the noise, $\hat{\sigma}$, is found as the intersection between the linear regression of the data set corresponding to homogenous areas with the ordinate ( $y$ ) axis.

### 3.1.2 Data masking method (DM)

DM method deals by first filtering the image to remove the image structure, leaving only the noise (Corner et al., 2003). The Laplacian Kernel presented in equation.9 is used for that purpose. The image obtained after the convolution with the Laplacian kernel (Laplacian image) mainly contains the noise as well as the edges of the objects present in the original image. The Laplacian image is further filtered with a Sobel detector (Kazakova et al., 2004), followed by a threshold in order to create a binary edge map. This edge map is subtracted to the Laplacian image (to produce the Final Image) in order to reduce the contribution of the edges to the noise estimation.

The optimal threshold is established by varying the threshold and choosing the one for which the variance in the final image (Laplacian – edge map) is maximum

Then, on the final image, standard deviations are calculated on 9x9 blocks and the median value of the histogram of the standard deviation is used as the estimate of the noise standard deviation.

$$L = \begin{pmatrix} 1 & -2 & 1 \\ -2 & 4 & -2 \\ 1 & -2 & 1 \end{pmatrix} \tag{9}$$

The outline of the noise estimation procedure can be summarized by the following algorithm:

1-Start
2-Acquire Image
3-Apply Laplacian Kernel
4-Apply Sobel Kernel
5-Select the optimal threshold
6-Subtract edges map to the Laplacian Image
7-Calculate the variance in a 9x9 blocks
8-Create the histogram of the standard deviation
9-Select the median value as the noise standard deviation estimate.
10-Stop

### 3.2 Fractal vectorization filtering algorithm (FVFA)

The two previous methods have limitations which can be summarized as follows:

- SP method is not appropriate for rich textured images. It is time effective because of the calculation of local statistics within the image.
- DM method overestimates the noise parameters due to edges points which remain in the final image.

In order to estimate the final noise parameters, our algorithm keeps the idea of calculating the residual image and the use of the local statistics. The remaining limitations of these combined ideas will be compensated by a vectorization of the residual image by the Peano-Hilbert fractal path.

As for the DM method, operations 1 to 6 (with a fixed filter) are applied to the original image. The resulting image is then transformed on a vector following a fractal path as presented in an $9 \times 9$ image example of Figure.3. The path deals with the Peano-Hilbert

fractal path and the vector is designed in the same way as the numbering of Figure.3, from 1 to 81.

| | | | | | | | | |
|---|---|---|---|---|---|---|---|---|
| 1 | 6 | 7 | 48 | 49 | 54 | 55 | 60 | 61 |
| 2 | 5 | 8 | 47 | 50 | 53 | 56 | 59 | 62 |
| 3 | 4 | 9 | 46 | 51 | 52 | 57 | 58 | 63 |
| 16 | 15 | 10 | 45 | 40 | 39 | 70 | 69 | 64 |
| 17 | 14 | 11 | 44 | 41 | 38 | 71 | 68 | 65 |
| 18 | 13 | 12 | 43 | 42 | 37 | 72 | 67 | 66 |
| 19 | 24 | 25 | 30 | 31 | 36 | 73 | 78 | 79 |
| 20 | 23 | 26 | 29 | 32 | 35 | 74 | 77 | 80 |
| 21 | 22 | 27 | 28 | 33 | 34 | 75 | 76 | 81 |

Fig. 3. Peano-Hilbert fractal path

Local means $\mu$ and standard deviations $\sigma$ are calculated on the resulting vector by using a shifting interval. The local mean and non-biased standard deviation are respectively defined as:

$$\mu_v(i) = \frac{1}{2m+1} \sum_{k=-m}^{m} v(i+k) \tag{10}$$

$$\sigma_v(i) = \left( \frac{1}{2m} \sum_{k=-m}^{m} (v(i+k) - \mu_v(i))^2 \right)^{1/2}$$

where $v$ is the portion of the Laplacian image vector limited by the shifting interval of size $2m+1$. These local statistics are the vectorial version of those calculated in SP algorithm applied on the residual no-edges image.

The plane $(\mu, \sigma)$ is then plotted. Two types of points are formed in that plane (Aiazzi et al., 2002). The first type is a dense cloud and the second is an isolated set of points corresponding to the remaining edges pixels that are not eliminated by the Sobel filtering. The intersection of linear regression of the cloud points and the $y$ axis gives the better estimation of the noise standard deviation. Similarly, the mean of the noise may be estimated by applying the same instructions on the plotted plane $(\sigma, \mu)$.

The advantage of the fractal path is double: it eases the task of calculating the local statistics within the image with keeping at most the neighbourhood of image pixels. Moreover, the vectorization of the image disperses so much the isolated points of the plane $(\mu, \sigma)$

preventing the regression process from taking them into account. This fact decreases the overestimation of the noise as in the DM method.

### 3.3 Application to gray level images

To prove the efficiency of the proposed algorithm, three experiments were carried out on two 256x256 gray level images (Figure.4). The first image is a chessboard image and the second image is a section of the 3D MRI (Magnetic Resonance Imaging) of the head. Additive noises of zero mean with variances 5, 10, 30 and 60 are added to these two images. The noise variance is then estimated by the three methods exposed previously: SP method, DM method, and our proposed algorithm (FVFA). In order to have robust statistical results, the estimated standard deviation $\hat{\sigma}$ is the empirical mean of 200 estimations found by the re-sampling Bootstrap method (Cheng, 1995). The dispersion $\sigma_d$ is then estimated showing that the exact value of the standard deviation lies in the interval $\left[\hat{\sigma}-3\sigma_d, \hat{\sigma}+3\sigma_d\right]$ with a probability of 99,73%.

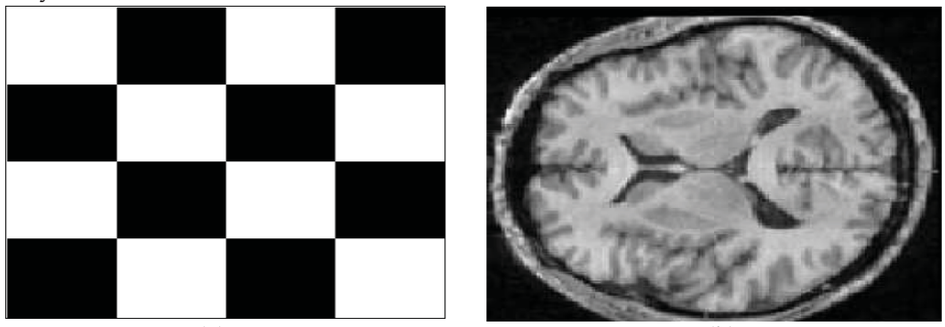

(a) (b)

Fig.4. Gray level images used to the validation of the proposed algorithm, (a) chessboard, (b) section of a 3D MRI of the head.

The results of the estimation are summarized in Table 1 for the Figure.4. (a) and in Table 2 for the Figure. 4. (b). The dispersion $\sigma_d$ is displayed between brackets.

Our algorithm proved to exhibit better performances than the two other methods. As expected our method is even better when dealing with textured image (table 1).

Combined with some physical considerations, in the next section this method is applied to estimate the noise present in polarimetric images.

| Simulated noise | SP method | DM method | FV method |
|---|---|---|---|
| $\sigma^2$ | $\hat{\sigma}^2$ | $\hat{\sigma}^2$ | $\hat{\sigma}^2$ |
| 5 | 10.23[0.5] | 9.3[0.41] | 5.8[0.04] |
| 10 | 16.84[0.45] | 11.45[0.32] | 10.97[0.02] |
| 30 | 35.09[0.3] | 32.75[0.27] | 29.59[0.01] |
| 60 | 63.75[0.27] | 62.04[0.12] | 60.75[0.01] |

Table 1 – Comparison of the noise estimation parameters using SP, DM and FVFA methods on the image of Figure.4. (a).

| Simulated noise | SP method | DM method | FV method |
|---|---|---|---|
| $\sigma^2$ | $\hat{\sigma}^2$ | $\hat{\sigma}^2$ | $\hat{\sigma}^2$ |
| 5 | 9.13[0.48] | 7.8[0.41] | 5.4[0.01] |
| 10 | 13.12[0.41] | 11.23[0.3] | 9.38[0.01] |
| 30 | 32.45[0.29] | 31.01[0.15] | 30.25[0.009] |
| 60 | 57.41[0.16] | 61.08[0.2] | 60.09[0.007] |

Table 2 – Comparison of the noise estimation parameters using SP, DM and FVFA methods on the image of Figure. 4. (b).

## 4. Polarimetric images filtering

### 4.1 Polarization-based filtering

As seen in section 2 the measured Stokes vector $\hat{S}$ attached to the pixel $(i, j)$ is given as an independent sum of the perfect Stokes vector $S_p$ and an attached noise term $\delta S$ by:

$$\hat{S}(i,j) = S_p(i,j) + \delta S(i,j) \tag{11}$$

The term $\delta S$ is equal to $A^{-1}\delta I$ ($\delta I = n_a$). Under Gaussian assumption of the additive noise, noise parameters are estimated by FVFA method. The intensity noise $\delta I$ is reconstructed and the polarimetric noise attached term $\delta S$ is calculated.

Naturally, the real Stokes vector $S_p$ can be derived from equation (11) by:

$$S_p(i,j) = \hat{S}(i,j) - \delta S(i,j) \tag{12}$$

Furthermore, the richness information of our images is extremely conditioned by the physical content, .i.e. the vector $S_p$ must satisfy equation (2). However, the direct application of equation (12) to filter polarimetric image may induce the non physical

behaviour of a large amount of image pixels. Mathematically, this is due to the fact that the set of physical Stokes vectors is not a space vector. Therefore, any addition or subtraction of two Stokes quantities may lead to a no physical result.
In order to handle this fundamental limitation, a new tool is needed to find the best trade-off between the filtering and the physical constraint of Stokes images.
The Stokes vector $S_p$ must satisfy equation (2), which is equivalent to the following formula:

$$S_p^T G S_p \geq 0, \qquad G = diag(1,-1,-1,-1) \tag{13}$$

Where $diag$ refers to the diagonal. To control the physical condition on the vector $S_p$, a parameter $\alpha$ which lies in the interval $[0,1]$ is inserted into equation (12) such that:

$$S_p = \hat{S} - \alpha \delta S \tag{14}$$

If this parameter is too large the physical condition will not be respected whereas if it is too small the filtering is not efficient. The parameter $\alpha$ cannot take negative values; it will result in noise amplification.
Combining equations (13) and (14), one has to search the parameter $\alpha$ that satisfies:

$$\left(\hat{S} - \alpha \delta S\right)^T G \left(\hat{S} - \alpha \delta S\right) \geq 0 \tag{15}$$

Developing equation (15), one has to search the parameter $\alpha$ that respects the inequality:

$$\begin{aligned} f(\alpha) &= \left(\hat{S} - \alpha \delta S\right)^T G \left(\hat{S} - \alpha \delta S\right) = \\ &\hat{S}^T G \hat{S} - \left(\delta S^T G \hat{S} + \hat{S}^T G \delta S\right)\alpha + \left(\delta S^T G \delta S\right)\alpha^2 \geq 0 \end{aligned} \tag{16}$$

Assuming that $a = \delta S^T G \delta S$, $b = \delta S^T G \hat{S} + \hat{S}^T G \delta S$, $c = \hat{S}^T G \hat{S}$, equation (16) is written in the simplified form as:

$$f(\alpha) = a\alpha^2 + b\alpha + c \geq 0 \tag{17}$$

Two real solutions are given by:

$\alpha = \dfrac{-b - \sqrt{\Delta}}{2a}$, $or$ $\alpha = \dfrac{-b + \sqrt{\Delta}}{2a}$, with $\Delta = b^2 - 4ac$

Assume that $\alpha_1$ always refers to the smallest solution and $\alpha_2$ to the greatest one. For an infinitesimal $\varepsilon$ such that if $\alpha_i$ is positive, $\alpha_i - \varepsilon$ is still positive and after the classical resolution of the inequality (17), three cases arise depending on the sign of $a$:

$sign(a) > 0$

- If $1 \in [\alpha_1, \alpha_2]$ thus $\alpha = 1$
- If $1 \in [\alpha_1, \alpha_2]$ and $\alpha_1 > 0$ thus $\alpha = \alpha_1 - \varepsilon$
- Otherwise there is no $\alpha$ between 0 and 1

$sign(a) < 0$

- If $1 \in [-\infty, \alpha_1] \cup [\alpha_2, +\infty]$ thus $\alpha = 1$
- If $0 < \alpha_2 < 1$ thus $\alpha = \alpha_2 - \varepsilon$

- Otherwise there is no $\alpha$ between 0 and 1

$a = 0$

- One solution exists $\alpha_1 = \alpha_2 = \frac{c}{b}$
- If $0 < \alpha_1 < 1$ thus $\alpha = \alpha_1 - \varepsilon$
- If $\alpha_1 > 1$ thus $\alpha = 1$
- Otherwise there is no $\alpha$ between 0 and 1

These three cases take in account the fact that $\alpha$ must belong to [0,1]. Finally the algorithm can be summarized as:

1. Construct the noise term $\delta S$ attached to each image pixel by the FVFA method Compute equation (10) for each pixel
2. If the pixel's Stokes vector is physically realisable (equation (2) verified for the pixel), set $\alpha$ to 1
3. Otherwise, search the parameter $\alpha$ by following the above instructions.
4. If the discriminate $\Delta$ is negative or if there is no $\alpha$ in [0,1], choose the Stokes vector satisfying the maximum between $\hat{S}^T G \hat{S}$ and $S_p^T G S_p$

### 4.2 Illustration and discussion

Our algorithm is run on two images: one simulated Stokes image for which the noise additive contents is known and a real Stokes image. The synthetic image is built as follows: the Stokes vector at the image center is set to $S = \begin{bmatrix} 1 & 1/\sqrt{3} & 1/\sqrt{3} & 1/\sqrt{3} \end{bmatrix}$ (white elliptical part) and to zero elsewhere. Stokes images are multiplied by the modulation matrix $A$ as in equation (3) in order to have the corresponding intensity channels. Then, a Gaussian noise of zero mean and variance 0.2 is added to each intensity channel. Noisy images are inverted as in equation (7) to get the noisy Stokes image (Figure. 5).

The estimated variances using FVFA filtering algorithm on the four intensity channels corresponding to $S_0, S_1, S_2$ and $S_3$ are respectively 0.18, 0.19, 0.194 and 0.187.

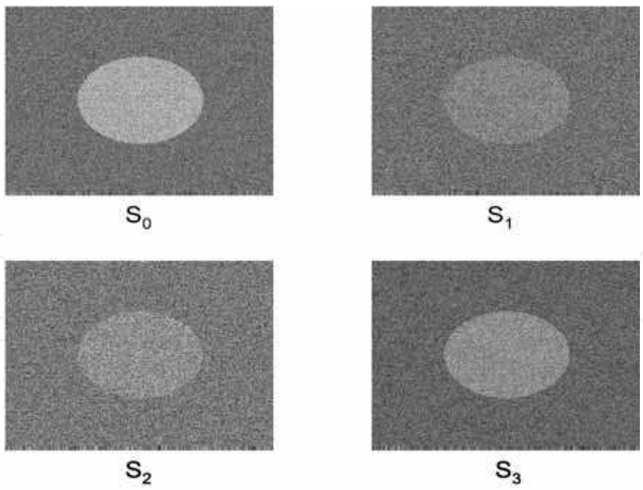


Fig. 5 . Noisy Stokes channels. Gaussian zero-mean noise and of variance 0.2 is added to the correspondent intensity channels

These values are very close to the simulated variance. The results also show that the noise affecting the four polarimetric measurements is roughly the same. The regularization parameter $\alpha$ is calculated for each pixel. Figure. 6 shows the binary values of this parameter. Pixels for which $\alpha$ is found between 0 and 1 appear white otherwise black.

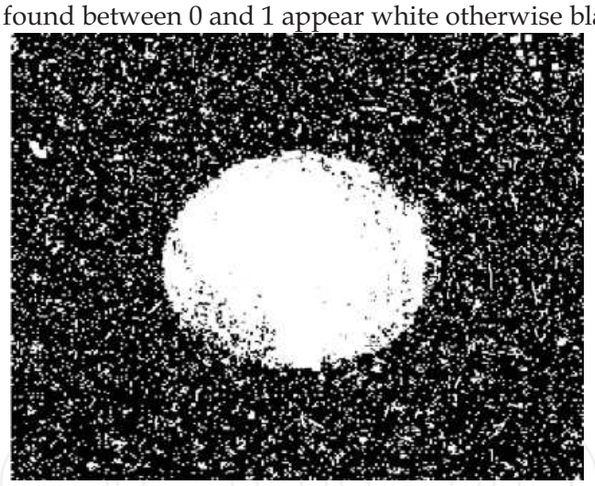

Fig. 6. Binary values of the regularization parameter $\alpha$

The use of the regularization parameter allows the processing of an important amount of pixels in the image. Indeed without this parameter (equation 12), the image is well filtered but only 10% of the pixels in $S_p$ have physical meaning whereas it reaches 70% with the use of parameter $\alpha$ (equation 14). The amount of remaining pixels having no physical meaning is less important. It is due to the fact that conditions 1 to 4 of the algorithm are not satisfied and neither $\hat{S}^T G \hat{S}$ nor $S_p^T G S_p$ are positive (step 4). The result of the two filtering processes is illustrated in Figure. 7.

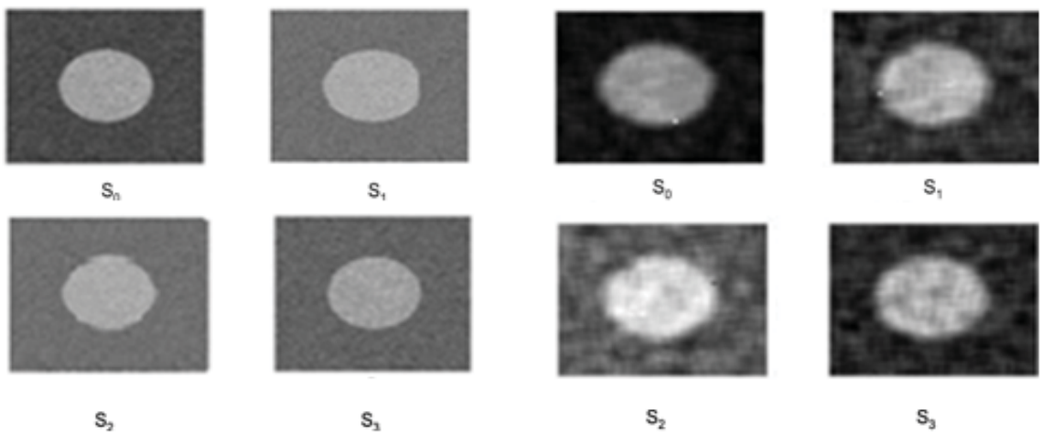


(a) (b)

Fig.7. Filtered Stokes images with: (a) regularization parameter (equation 10), (b) without regularization parameter (equation 12)

As shown in Figure.7. (a), our algorithm ensures an improvement in polarimetric information carried by Stokes image preserving its physical constraint for most of the pixels. The real measurement case deals with the Stokes image of Figure. 2. The inherent noise variances estimated on the correspondent intensity images are respectively up to 10.75, 10.52, 9.78 and 9.88 on a gray scale value of 8 bits. Results of the physical filtering on noisy Stokes images are presented in Figure. 8. The new filtering ensures 64% of physical pixels whereas the classical filtering ensures only 7% of physical pixels. Again, real experiment shows the performances of our method. The proposed algorithm is thus a trade-off between a fully filtered image and a physical constrained (of the most pixels) image. Only additive independent noie is considered herein. Consequently, most of the imperfections remaining after the physical filtering (Figure. 8. b) arise from other sources of noise. This problem will be addressed in future works.

## 5. Conclusion

A new algorithm to filter polarimetric images is introduced in this chapter. Based on the filtering methods of multispectral images and combined with a fractal vectorization of the image, the new algorithm is a trade-off between a classical filtering (noise smoothing) and preserving the physcial meaning of the data. No comparison with other methods is done in this paper, because in the best of our knowledge, this work is the first dealing with the trade-off between filtering of polarimetric images and preserving the physical condition. Our methods are tested on simulated and on real images acquired with a classical polarimeter. Promising results were presented at the end of the chapter. As the additive noise in not the only noise affecting polarimetric measurement, other sources of noise are currently being investigated especially multiplicative noise.

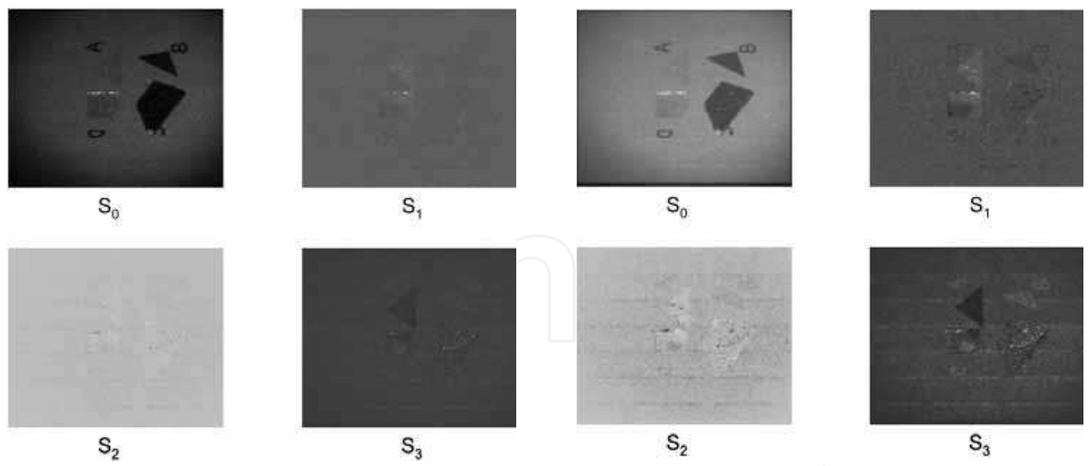


(a) (b)

Fig. 8. (a) Noisy Stokes image, (b) Filtered Stokes image

## 6. References

B. Aiazzi, L. Alparone, A. Barducci, S. Baronti & I. Pippi. (2002). Estimating noise and information of multispectral imagery, In *Opt. Eng*, vol.41, pp. 656–668.

S. Ainouz, J. Zallat & A. De Martino. (2006a). Clustering and color preview of polarization-encoded images. *Eusipco 2006*, Firenze, September 2006, Italy.

S. Ainouz, J. Zallat, A. De Martino & C. Collet. (2006b). Physical interpretation of polarization-encoded images by color preview, *Opt. Express*, Vol. 14, pp. 5916-5927.

A. Bénière, F. Goudail, M. Alouini & D. Dolfi. (2007). Precision of degree of polarization estimation in the presence of additive Gaussian detector noise, *Optics Communication*, vol. 278, pp. 264–269, October 2007.

R. C. H. Cheng. (1995). Bootstrap methods in computer simulation experiments, in *Simulation Conference Proc*. vol.2, pp. 71–177.

R.A. Chipman. (1993). Polarimetry, In: *Handbook of Optics*, M. Bass, ed (McGraw-Hill, New York), pp. 22.1-22.36.

A. B. Corner, R. M. Narayanan & S. E. Reichenbach. (2003). Noise estimation in remote sensing imagery using data masking, In *Int. J. Remote sensing*, vol.4, pp. 689–702.

M. Ferraton, C. Stolz & F. Meriaudeau. (2007). 3D reconstruction of transparent objects using image polarization, *EOS topical meeting*, pp. 110-111, Lille, France.

N. Kazakova, M. Margala & N. G. Durdle. (2004). Sobel edge detection processor for a real-time volume rendering system, in *ISCAS'04*, vol.2, pp. 913–916.

M. Miura et al. (2006). Imaging Polarimetry in Central Serous Chorioretinopathy, *American Journal of Ophtamology*, 40 (6), pp. 1014-1019.

O. Morel, C. Stolz, F. Meriaudeau & P. Gorria. (2006). Active Lighting Applied to 3D Reconstruction of Specular Metallic Surfaces by Polarization Imaging, *Applied Optics*, 45 (17), pp. 4062-4068

S. Tyo, et al. (2006). Review of passive imaging polarimetry for remote sensing applications, Vol. 45, No. 22 , *Applied Optics*, pp 4553-5469.

J. Zallat, S. Ainouz & M-P. Stoll. (2006). Optimal configuration for imaging polarimeters : impact of image noise and systematic errors, in *J. Opt.* vol.8, pp. 807–814.

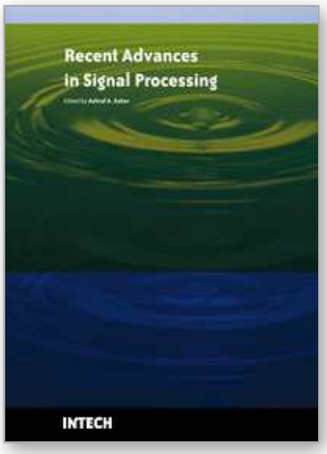


**Recent Advances in Signal Processing**

Edited by Ashraf A Zaher

ISBN 978-953-307-002-5

Hard cover, 544 pages

**Publisher** InTech

**Published online** 01, November, 2009

**Published in print edition** November, 2009

The signal processing task is a very critical issue in the majority of new technological inventions and challenges in a variety of applications in both science and engineering fields. Classical signal processing techniques have largely worked with mathematical models that are linear, local, stationary, and Gaussian. They have always favored closed-form tractability over real-world accuracy. These constraints were imposed by the lack of powerful computing tools. During the last few decades, signal processing theories, developments, and applications have matured rapidly and now include tools from many areas of mathematics, computer science, physics, and engineering. This book is targeted primarily toward both students and researchers who want to be exposed to a wide variety of signal processing techniques and algorithms. It includes 27 chapters that can be categorized into five different areas depending on the application at hand. These five categories are ordered to address image processing, speech processing, communication systems, time-series analysis, and educational packages respectively. The book has the advantage of providing a collection of applications that are completely independent and self-contained; thus, the interested reader can choose any chapter and skip to another without losing continuity.



**InTech Europe**
University Campus STeP Ri
Slavka Krautzeka 83/A
51000 Rijeka, Croatia
Phone: +385 (51) 770 447
Fax: +385 (51) 686 166
www.intechopen.com

**InTech China**
Unit 405, Office Block, Hotel Equatorial Shanghai
No.65, Yan An Road (West), Shanghai, 200040, China
中国上海市延安西路65号上海国际贵都大饭店办公楼405单元
Phone: +86-21-62489820
Fax: +86-21-62489821

IntechOpen